

The theory of synchrotron emission from supernova remnants[★]

E. G. Berezhko¹ and H. J. Völk²

¹ Institute of Cosmophysical Research and Aeronomy, 31 Lenin Av., 677891 Yakutsk, Russia
e-mail: berezhko@ikfia.ysn.ru

² Max Planck Institut für Kernphysik, Postfach 103980, 69029 Heidelberg, Germany
e-mail: Heinrich.Voelk@mpi-hd.mpg.de

Received 16 April 2004 / Accepted 9 July 2004

Abstract. The time-dependent nonlinear kinetic theory for cosmic ray (CR) acceleration in supernova remnants (SNRs) is applied studying the properties of the synchrotron emission from SNRs, in particular, the surface brightness-diameter ($\Sigma - D$) relation. Detailed numerical calculations are performed for the expected range of the relevant physical parameters, namely the ambient density and the supernova explosion energy. The magnetic field in SNRs is assumed to be significantly amplified by the efficiently accelerating nuclear CR component. Due to the growing number of accelerated CRs the expected SNR luminosity increases during the free expansion phase, reaches a peak value at the beginning of the Sedov phase and then decreases again, since in this stage the overall CR number remains nearly constant, whereas the effective magnetic field diminishes with time. The theoretically predicted brightness-diameter relation in the radio range in the Sedov phase is close to $\Sigma_R \propto D^{-17/4}$. It fits the observational data in a very satisfactory way. The observed spread of Σ_R at a given SNR size D is the result of the spread of supernova explosion energies and interstellar medium densities.

Key words. X-rays: stars – stars: supernovae: general – shock waves – acceleration of particles – radiation mechanisms: non-thermal – magnetic fields

1. Introduction

Supernova remnants (SNRs) are the main sources of energy for the Interstellar Medium (ISM). They also control the physical state of the ISM which presumably includes the nonthermal component of Interstellar matter, often called the Galactic Cosmic Rays (CRs). The synchrotron emission of relativistic electrons plays an important role in the general study of SNR properties and in CR production inside SNRs in particular. All known SNRs are sources of radio-synchrotron emission. Several Galactic SNRs were recently detected as sources of nonthermal X-ray emission which is presumably also of synchrotron origin (e.g. Petre et al. 2001).

The determination of the distances to the Galactic SNRs is an important task which is often based on radio observations. When there is no direct distance determination, estimates can be made by using the radio surface brightness-to-diameter relationship ($\Sigma_R - D$). It is however not clear whether any functional correlation between $\Sigma_R(t)$ and $D(t)$ exists for individual objects during their evolution in time t , and if so, for which physical reason (Green 1984; Case & Bhattacharya 1998).

CRs are widely accepted to be produced in SNRs by the diffusive shock acceleration process at the outer blast wave (see e.g. Drury 1983; Blandford & Eichler 1987; Berezhko & Krymsky 1988, for reviews). The nonlinear kinetic theory

of diffusive CR acceleration in SNRs (Berezhko et al. 1996; Berezhko & Völk 1997) is able to make quite definite predictions about the energy spectrum and the spatial distribution of CR nuclei and electrons at any given evolutionary epoch t , and about the properties of the nonthermal radiation produced in SNRs due to these accelerated CRs. Application of this theory to individual SNRs (Berezhko et al. 2002, 2003a,b; Völk et al. 2002) has demonstrated its power in explaining the observed SNR properties and in predicting new effects like magnetic field amplification, leading to the concentration of the highest-energy electrons in a very thin shell just behind the shock. At the same time there does not yet exist a systematic study of the synchrotron emission expected during the different evolutionary epochs of SNRs, possibly leading in particular to a $\Sigma_R - D$ relation. An interesting question is specifically whether or not the observed $\Sigma_R - D$ relation corresponds to the evolutionary track of a single typical SNR, as was for example argued by Duric & Seaquist (1986). Such a study is the aim of the present paper.

Previous considerations (e.g. Reynolds & Chevalier 1981; Duric & Seaquist 1986; Huang et al. 1994) show that to explain on average the observed radio synchrotron emission one needs magnetic fields inside SNRs that are much higher than those corresponding to typical ISM values, $B_{\text{ISM}} \approx 5 \mu\text{G}$. The Rayleigh-Taylor instability of the contact discontinuity, separating ejecta and swept-up ISM, has been considered as a possible mechanism of magnetic field amplification in

[★] Appendix is only available in electronic form at <http://www.edpsciences.org>

SNRs (Gull 1973; Fedorenko 1983; Duric & Seaquist 1986). However, it is unlikely that electrons which are accelerated at the outer blast wave and produce radio emission can penetrate so deeply into the interior where the magnetic field is amplified due to this instability. The typical energies of such radio electrons is so small that their diffusion coefficient is several orders of magnitude less than $R_s V_s$, the product of shock radius and shock speed. This means that these electrons are strongly tied to the downstream medium and that their diffusion is not important. To play a role in the synchrotron emissivity of SNRs, magnetic field amplification should occur in the same region where also the energetic electrons are produced, that is at the shock front. Assuming such a scenario Reynolds & Chevalier (1981) concluded that several percent of the shock energy should be converted into (amplified) magnetic field energy to explain the observed properties of the radio emission during the Sedov phase. If the magnetic field was not amplified, the expected time dependence of the SNR synchrotron emissivity did not fit the observations.

On the other hand, Luceck & Bell (2000) came to the conclusion that a strong magnetic field amplification near the shock can indeed be produced nonlinearly by a very efficiently accelerated nuclear CR component. In this case the CR energy content and streaming anisotropy along the field is so high that magnetohydrodynamic waves can be strongly excited, amplifying the magnetic field already upstream of the shock, where the CR distribution is characterized by a large spatial gradient. In addition, detailed observational evidence has been obtained regarding the spatial fine structure of nonthermal X-rays in young SNRs (Hwang et al. 2002; Vink & Laming 2003; Long et al. 2003; Bamba et al. 2003), which can be explained only if the magnetic field at the outer shock and inside SNRs is indeed strongly amplified (Berezhko et al. 2003a; Berezhko & Völk 2004).

In the following we shall present a detailed study of the evolutionary properties of the synchrotron emission of SNRs. There are a number of distinct differences between the present and previous studies: (i) our approach is based on the nonlinear kinetic theory self-consistently taking into account the backreaction of the accelerating CRs on the SN shock structure and remnant dynamics (ii) to reproduce the evolution of the synchrotron emission we calculate self-consistent electron spectra which take the synchrotron losses into account. This is done for every SNR evolutionary stage starting from the very early time after the SN explosion up to the late Sedov phase when the SN shock already becomes an inefficient accelerator (iii) we take into account magnetic field amplification near the outer SN shock due to CR backreaction on the thermal plasma and its magnetic field (iv) to explain the spread of the observed properties of the SNR synchrotron emission we perform our calculations for different values of the relevant physical parameters such as SN explosion energy and ISM density (v) since recently X-ray synchrotron emission was detected for a number of SNRs, we study here the expected properties of the SNR synchrotron emission for the entire wavelength range, from the radio to the X-ray band.

2. Model

A supernova explosion ejects an expanding shell of matter with total energy E_{sn} and mass M_{ej} into the surrounding ISM. During an initial period the shell material has a broad distribution in velocity v . The fastest part of these ejecta is described by a power law

$$dM_{\text{ej}}/dv \propto v^{2-k} \quad (1)$$

with $k = 7$ to 12 (e.g. Jones et al. 1981; Chevalier 1982). The interaction of the ejecta with the ISM creates a strong shock which accelerates particles. We note that more recently also exponential profiles for the velocity distribution of the ejecta have been discussed (Dwarkadas & Chevalier 1998). However we believe that for the global synchrotron emission the differences between these different approximations are not significant. Thus we use here the power-law ansatz above.

Our nonlinear model (Berezhko et al. 1996; Berezhko & Völk 1997) is based on a fully time-dependent solution of the CR transport equation together with the gas dynamic equations in spherical symmetry. Since all relevant equations, initial and boundary conditions for this model have already been described in detail elsewhere (Berezhko et al. 1996; Berezhko & Völk 1997; Berezhko & Ksenofontov 1999), we do not present them here and only briefly discuss the most important aspects below.

Due to the streaming instability CRs efficiently excite large-amplitude magnetic fluctuations upstream of the SN shock (e.g. Bell 1978; Blandford & Ostriker 1978; McKenzie & Völk 1982). Since these fluctuations scatter CRs extremely strongly, the CR diffusion coefficient is assumed to be as small as the Bohm limit

$$\kappa(p) = \kappa(mc)(p/mc), \quad (2)$$

where $\kappa(mc) = mc^3/(3eB)$, e and m are the particle charge and mass, p denotes the particle momentum, B is the magnetic field strength, and c is the speed of light.

If B is the pre-existing field in the surrounding ISM, then the Bohm limit implies that the instability growth is restricted by some nonlinear mechanism to the level $\delta B \sim B$, where δB is the wave field. The attempt to give a nonlinear description of the magnetic field evolution in a numerical model (Luceck & Bell 2000) ended in the conclusion that a considerable field amplification should occur, resulting in what we call the effective magnetic field. Broadly speaking, it was expected that a significant fraction of the shock ram pressure $\rho_0 V_s^2$ (ρ_0 is the ISM density, V_s is the shock speed) would be converted into magnetic field energy (Bell & Luceck 2001).

At the same time, from an analysis of the synchrotron spectrum of SN 1006 (Berezhko et al. 2002), Cassiopeia A (Berezhko et al. 2003b) and Tycho's SNR (Völk et al. 2002) such a strong magnetic field amplification can only be produced as a nonlinear effect by a very efficiently accelerated nuclear CR component. Its energy density, consistent with all existing data, is so high that it is able to strongly excite magnetohydrodynamic fluctuations, and thus to amplify the upstream magnetic field B_{ISM} to an effective field $B_0 > B_{\text{ISM}}$, and at the

same time to permit efficient CR scattering on all scales, approaching the Bohm limit. The same large effective magnetic field is required by the comparison of our self-consistent theory with the *morphology* of the observed X-ray synchrotron emission, in particular, its spatial fine structure (Berezhko et al. 2003a; Berezhko & Völk 2004).

As the simplest possible conclusion from these independent but convergent considerations we shall assume that a constant fraction δ of the CR pressure P_c at the shock is converted into magnetic field energy so that $B^2/(8\pi) = \delta \cdot P_c$. Formally then, the magnetic field in the upstream preshock medium becomes time dependent, independent of the magnetic field in the ambient interstellar medium around the SNR:

$$B_0 = \sqrt{8\pi\delta \cdot P_c}. \quad (3)$$

We use the moderate parameter value $\delta = 10^{-3}$. In the active SNR phase, when $P_c \sim \rho_0 V_s^2$, this results in an effective downstream magnetic field of energy density

$$B_d^2/(8\pi) \approx 10^{-2} \rho_0 V_s^2. \quad (4)$$

Such a large downstream magnetic field value is consistent with the values derived from the nonthermal X-rays measured in individual SNRs (Berezhko et al. 2003a; Berezhko & Völk 2004). When in the course of SNR evolution this field value drops below the magnetic field value B_{ISM} in the ambient ISM, we shall use $B_0 = B_{\text{ISM}} = 5 \mu\text{G}$. Note that this amplified magnetic field B_0 exceeds the typical ISM value $B_{\text{ISM}} \approx 5 \mu\text{G}$ during almost the entire evolution except in the very late SNR evolutionary phase. Therefore the results of our calculations below are insensitive to the concrete value of B_{ISM} .

To a good approximation the amplified field $B_d(r, t)$ in the downstream region is spatially uniform and equal to its value $B_2(t)$ just behind the shock (see Appendix). This is also roughly true for the free expansion phase. For simplicity in what follows we shall make use of this property for all evolutionary epochs considered.

The number of suprathermal protons injected into the acceleration process is described by a dimensionless injection parameter η which is a fixed fraction of the number of ISM particles entering the shock front. For simplicity assume that the injected particles have a velocity equal to four times the post-shock sound speed. Note that the value of the injection velocity v_{inj} is not a significant parameter. Since it divides the whole particle distribution into two physically different components, thermal particles and energetic particles (which we call here cosmic rays), the only significant requirement for the value v_{inj} is that it should be high enough, so that the diffusive approach is valid for all energetic particles (for a detailed discussion, see Malkov & Völk 1995). For a given value v_{inj} the only relevant parameter which determines the number of suprathermal particles injected into the acceleration is the injection parameter η .

Assuming a purely parallel shock, η is estimated to be $\eta \approx 10^{-2}$ (e.g. Scholer et al. 1992; Malkov 1998). As analyzed in detail by Völk et al. (2003) the directional structure of the fluctuating magnetic field at the shock front has the effect of increasingly suppressing the leakage of suprathermal particles from the downstream region back upstream when the shock becomes instantaneously more and more oblique. Applied to the

spherical SNR shock in a large-scale external field B_{ISM} , the local injection rate averaged over the fluctuating magnetic field directions is lower than for a purely parallel shock by a factor $\approx 10^{-2}$, and even this reduced injection takes place only on some fraction $f_{\text{re}} = 0.15$ to 0.25 of the shock surface, depending on the size of the SNR. Therefore we adopt here a value $\eta \sim 10^{-4}$ for the injection parameter and choose a renormalization factor $f_{\text{re}} = 0.2$. The latter is used to renormalize (reduce) the number of CRs calculated within our spherically symmetric model. These parameter values, used for the entire sample of SNRs discussed in this paper, are close to the values determined individually for the three objects SN 1006, Tycho's SNR, and Cas A, mentioned before. In detail the objects in the sample will naturally be somewhat different. Thus our theoretical analysis is expected to be appropriate for an entire population, even though it will not give a precise result for each individual object separately.

Since the proton injection rate is not known more precisely than by a factor of order unity, we compare the results of our calculations performed for $\eta = 10^{-4}$ with those corresponding to $\eta = 3 \times 10^{-4}$ in order to study the sensitivity of the calculations to the value of η .

It is assumed that also electrons are injected into the acceleration process at the shock front. Formally their injection momentum is taken to be the same as that of the protons. Since the details of the electron injection process are poorly known, we chose the electron injection rate such that the electron:proton ratio K_{ep} (which we define as the ratio of their distribution functions at all rigidities where the protons are already relativistic and the electrons have not yet been cooled radiatively) is a constant to be determined from the observations.

The electron dynamics is exactly the same as that for protons for electron rigidities corresponding to ultrarelativistic protons, as long as synchrotron losses are neglected. Therefore, beyond such rigidities and below the loss region the distribution function of accelerated electrons has the form

$$f_e(p) = K_{\text{ep}} f(p) \quad (5)$$

at any given time.

In the sequel we shall use a value $K_{\text{ep}} = 10^{-2}$ of the electron-to-proton ratio, similar to what is observed for the Galactic CRs. Only for sufficiently large momenta will the electron distribution function $f_e(p)$ deviate from this relation as a result of synchrotron losses. These are taken into account by supplementing the ordinary diffusive transport equation by a corresponding loss term:

$$\frac{\partial f_e}{\partial t} = \nabla \kappa \nabla f_e - \mathbf{w} \nabla f_e + \frac{\nabla \mathbf{w}}{3} p \frac{df_e}{dp} + \frac{1}{p^2} \frac{d}{dp} \left(\frac{p^3}{\tau_1} f_e \right), \quad (6)$$

where the first three terms on the right hand side describe diffusion, convection due to the mean gas speed \mathbf{w} , and adiabatic expansion/compression, respectively. The synchrotron loss time in the fourth term is given by the expression (e.g. Berezhinskii et al. 1990)

$$\tau_1 = \left(\frac{4r_0^2 B^2 p}{9m_e^2 c^2} \right)^{-1}, \quad (7)$$

where m_e is the electron mass and r_0 is the classical electron radius.

The solution of the transport equations for the energetic protons and electrons, and of the gas dynamic equations at each instant of time yields the CR spectra and the spatial distributions of CRs and thermal plasma. This makes it possible to calculate the expected nonthermal emission produced by CRs in SNRs.

The choice of K_{ep} allows one to determine the electron distribution function and to calculate the associated emission. The expected synchrotron SNR luminosity is given by the expression (e.g. Berezhinskii et al. 1990)

$$L_\nu = 3.8 \times 10^{-20} f_{re} \int_0^\infty dr r^2 B_\perp \int_0^\infty dp p^2 f_e(r, p, t) F\left(\frac{\nu}{\nu_c}\right) \quad (8)$$

in erg/(s Hz), where

$$F(x) = x \int_x^\infty K_{5/3}(x') dx', \quad (9)$$

$K_\mu(x)$ is the modified Bessel function, $\nu_c = 3eB_\perp p^2 / [4\pi(m_e c)^3]$, and B_\perp is the magnetic field component perpendicular to the line of sight. It yields the flux density S_ν at distance d :

$$S_\nu = L_\nu / (4\pi d^2). \quad (10)$$

Since in the shock region with efficient particle injection and acceleration the upstream magnetic field directions can be assumed to be almost completely randomized due to intense generation of magnetic fluctuations, we adopt the postshock magnetic field strength $B_2 = \sigma B_0$, taking into account that at the shock front the perpendicular field component undergoes MHD compression as a result of the gas compression. Below we shall use $B_\perp = 0.5B$.

3. Supernova dynamics

At the start our study, we assume for the SN explosion energy a typical value $E_{sn} = 10^{51}$ erg. We also restrict our consideration to the case of a uniform ISM and type Ia SNe which means $M_{ej} = 1.4 M_\odot$ and $k = 7$ (see Eq. (1)). Since the correlation between the SN sites and the ambient ISM density structure is not known we consider three different phases of the ISM with hydrogen number densities $N_H = 3, 0.3$ and 0.003 cm^{-3} , which determine the ISM mass density as $\rho_0 = 1.4m_p N_H$, where m_p is the proton mass. The numerical results for the time evolution of individual SNRs are shown in Fig. 1.

The gas dynamic part of the problem is characterized by the following length, time and velocity scales:

$$R_0 = (3M_{ej}/4\pi\rho_0)^{1/3}, \quad t_0 = R_0/V_0, \quad V_0 = \sqrt{2E_{sn}/M_{ej}},$$

which correspond to the sweep-up radius, the sweep-up time and the mean initial speed of the ejecta, respectively. The scaling values for the cases considered are $R_0 = 1.45, 3.2, 14.9$ pc and $t_0 = 166, 367, 1709$ yr, respectively.

We note that the following simplified approach is frequently used for the description of SNR dynamics. It treats

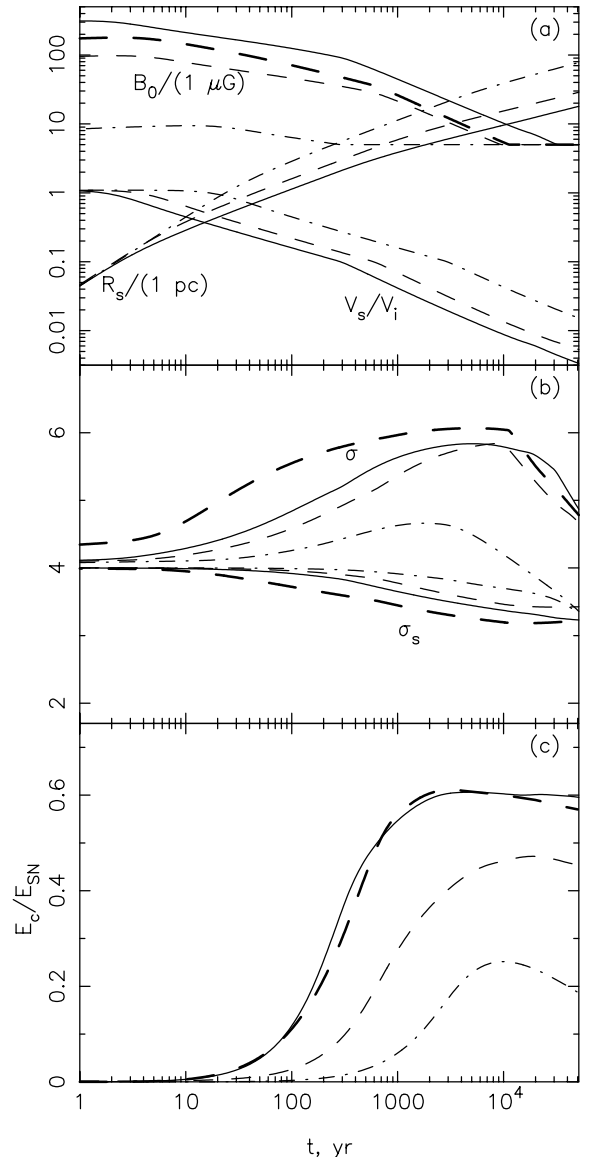


Fig. 1. Upstream effective magnetic field B_0 , shock radius R_s and shock speed V_s **a**); total shock (σ) and subshock (σ_s) compression ratios **b**); CR energy E_c as a function of time for the case of SN explosion energy $E_{sn} = 10^{51}$ erg and ISM gas number densities $N_H = 3 \text{ cm}^{-3}$ (solid lines), 0.3 cm^{-3} (dashed lines) and 0.003 cm^{-3} (dash-dotted lines) in the spherically symmetric case **c**). $V_i = 4 \times 10^4 \text{ km s}^{-1}$ is the initial piston speed. Thick dashed lines correspond to the case $E_{sn} = 10^{51}$ erg, $N_H = 0.3 \text{ cm}^{-3}$ with higher injection rate $\eta = 3 \times 10^{-4}$.

the ejecta as initially expanding as a whole with the single speed V_0 . In this case two different SNR evolutionary phases are distinguished: a free expansion phase with roughly constant shock speed $V_s \approx V_0$ (which lasts up to $t \approx t_0$) and the subsequent selfsimilar Sedov phase for $t > t_0$.

The actual ejecta, created after the SN explosion, have a broad distribution in velocity v , cf. Eq. (1). Due to this fact the SN shock undergoes substantial deceleration not only at $t > t_0$ but also at $t < t_0$. Despite this logical contradiction we shall still use below the term “free expansion phase” for the SNR evolution period corresponding to $t < t_0$.

As can be seen from Fig. 1, the shock speed is nevertheless constant during a short initial period. This occurs because we restrict the velocity distribution of the ejecta to a maximum speed $v_{\max} = 4 \times 10^4 \text{ km s}^{-1}$, which is also the initial speed of the outer part of the ejecta (piston) V_i . This period lasts up to the instant of time when the swept-up mass

$$M_{\text{sw}} = (4\pi/3)R_s^3\rho_0 \quad (11)$$

becomes equal to that part of the mass of the ejecta which has the initial speed $v = v_{\max}$. During this initial period the shock speed is $V_s = 1.1v_{\max}$.

During the subsequent part of the free expansion phase ($t < t_0$) the shock expansion law is

$$R_s \propto E_{\text{sn}}^{(k-3)/2k} M_{\text{ej}}^{(5-k)/2k} \rho_0^{-1/k} t^{(k-3)/k} \quad (12)$$

(Chevalier 1982) which for $k = 7$ gives

$$R_s \propto \left[E_{\text{sn}}^2 / (M_{\text{ej}}\rho_0) \right]^{1/7} t^{4/7}. \quad (13)$$

In the following adiabatic (Sedov) phase ($t \geq t_0$) we have

$$R_s \propto (E_{\text{sn}}/\rho_0)^{1/5} t^{2/5}. \quad (14)$$

The decelerating shock becomes progressively more modified, cf. Fig. 1b. The degree of shock modification is very well illustrated by the behavior of the shock compression ratios. When the CR pressure P_c is small compared to the ram pressure $\rho_0 V_s^2$ the shock is unmodified and has a compression ratio close to the classical value $\sigma = 4$. When P_c becomes comparable to $\rho_0 V_s^2$, CR backreaction leads to an increase of the total shock compression ratio σ , whereas the subshock compression ratio σ_s decreases. During an initial evolution period $t < 10^3 \text{ yr}$ the total shock compression ratio goes to the value, expected for a strongly modified shock (Berezhko & Ellison 1999)

$$\sigma \approx 1.5M_a^{3/8}, \quad (15)$$

where $M_a = V_s/c_{a0}$ is the shock Alfvén Mach number, $c_{a0} = B_0/\sqrt{4\pi\rho_0}$ is the Alfvén speed. This limit is achieved at the stage $t \approx 3 \times 10^3 \text{ yr}$. For example, in the case of $N_{\text{H}} = 3 \text{ cm}^{-3}$, $M_a \approx 30$ and $\sigma_{\text{max}} \approx 6$, in good agreement with the numerical results (Fig. 1b).

Since for $t = 10^3\text{--}10^4 \text{ yr}$ the amplified field $B_0 \propto V_s$, the Alfvén Mach number remains roughly constant. Therefore the shock modification is also nearly constant during this period of time (see Fig. 1b). When B_0 eventually becomes equal to B_{ISM} the Alfvén Mach number $M_a \propto V_s$ decreases and, according to Eq. (15), the shock compression ratio $\sigma \propto V_s^{3/8}$ also diminishes in time.

The non-renormalized CR energy content

$$E_c(t) = 16\pi^2 \int_0^\infty dr r^2 \int_0^\infty dp p^2 \epsilon_k f(r, p, t), \quad (16)$$

where $\epsilon_k = \sqrt{p^2 c^2 + m_p^2 c^4} - m_p c^2$ is the proton kinetic energy, increases during the SNR evolution up to the time $t \sim 10^4 \text{ yr}$, when the shock compression ratio starts to decrease rapidly to values $\sigma \sim 4$ and even less (Fig. 1c).

When the SNR age approaches $t \approx 10^5 \text{ yr}$, the CR acceleration efficiency also decreases as a result of the fall-off of the

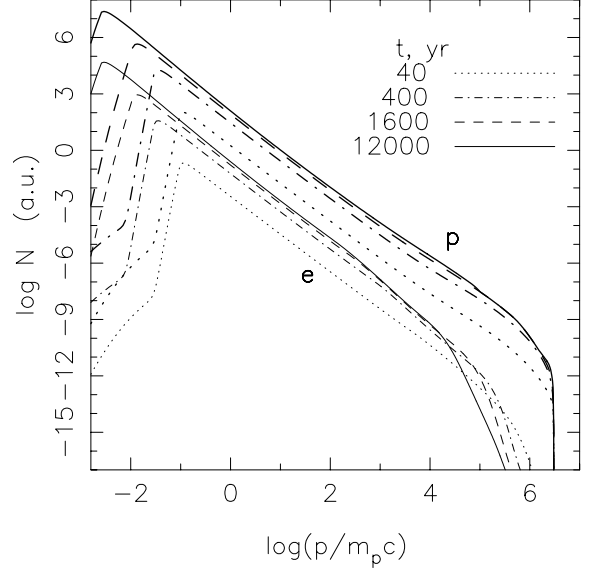


Fig. 2. The overall CR momentum spectrum for four different times, for the case of $E_{\text{sn}} = 10^{51} \text{ erg}$ and $N_{\text{H}} = 0.3 \text{ cm}^{-3}$. Thick and thin lines correspond to protons and electrons respectively.

Alfvén Mach number M_a . Due to its relatively low speed the shock at this stage continues to produce CRs albeit with relatively low cutoff momentum $p_m(t)$, whereas previously produced CRs with $p > p_m$ leave the shock volume since their diffusive propagation is now faster than that of the previously confining shock. This process of CR escape from the shock volume can be even faster in the case of strong Alfvén wave damping as a result of their nonlinear interaction (Ptuskin & Zirakashvili 2003). Therefore this late stage of the SNR evolution, $t \geq 3 \times 10^4 \text{ yr}$, does not play an important role in CR production, even though such an old SNR may still confine low energy CRs and shine in the radio range.

4. The accelerated CR distribution

4.1. Proton distribution

To illustrate the evolution of the accelerated CR spectrum we consider the case of $N_{\text{H}} = 0.3 \text{ cm}^{-3}$ and $E_{\text{sn}} = 10^{51} \text{ erg}$. The volume-integrated (or overall) CR distribution

$$N(p, t) = 16\pi^2 p^2 \int_0^\infty dr r^2 f(r, p, t) \quad (17)$$

for the CR proton and CR electron components is presented in Fig. 2 for different times. The amplitude of the spectrum increases with time roughly proportional to the CR energy content E_c . This process becomes very slow for $t > 10^3 \text{ yr}$ as seen from Fig. 2.

The maximum (or cutoff) momentum of the proton spectrum at a given evolutionary stage is determined by geometrical factors and can be estimated by the expression (Berezhko 1996)

$$\frac{p_m}{m_p c} = \frac{R_s V_s}{A \kappa (m_p c)}, \quad (18)$$

where

$$A = 4[2 + 2b + e - (\nu - 1)/\nu + d]. \quad (19)$$

The dimensionless parameters ν , e , b and d determine the time variation of the shock size $\nu = d \ln R_s / d \ln t$, of the diffusion coefficient $e = d \ln \kappa / d \ln t$, of the injection momentum $b = d \ln p_{\text{inj}} / d \ln R_s$, and of a measure of the inverse compression ratio $d = [2V_s - u + R_s(du/dr)]_2 / (u_1 - u_2)$. Here u is the plasma speed with respect to the shock front and the subscripts 1(2) correspond to the points just ahead (behind) the subshock front.

Let us consider the two SNR evolutionary periods when the SN shock is already strongly modified, i.e. the end of the free expansion phase and the Sedov phase. For a rough estimate one can take $P_c = 0.5\rho_0 V_s^2$. In the free expansion phase $\nu = 4/7$, $e = 3/7$, $b = -3/4$, $d = -1/2$. This gives $A = 5$ and

$$\frac{p_m}{m_p c} = 3.6 \times 10^6 \left(\frac{V_s}{10^4 \text{ km s}^{-1}} \right)^{2/3}. \quad (20)$$

In the Sedov phase we have $\nu = 2/5$, $e = 3/5$, $b = -3/2$, $d = 3$, which give $A = 16$ and

$$\frac{p_m}{m_p c} = 1.1 \times 10^6 \left(\frac{V_s}{10^4 \text{ km s}^{-1}} \right)^{4/3}. \quad (21)$$

The results presented in Figs. 1a and 2 agree very well with these estimates.

Since the most energetic CRs in the power law part of their spectrum are produced at the very end of the free expansion phase, that is at $t \sim t_0$, the maximum CR momentum depends on physical parameters as $p_{\text{max}} \propto V_0 R_0 B_0(t_0)$. This gives

$$\frac{p_{\text{max}}}{m_p c} \approx 10^6 \left(\frac{E_{\text{sn}}}{10^{51} \text{ erg}} \right) \left(\frac{M_{\text{ej}}}{1.4 M_\odot} \right)^{-2/3} \left(\frac{N_{\text{H}}}{0.3 \text{ cm}^{-2}} \right)^{1/6}, \quad (22)$$

where we have explicitly given the dependence on the SN parameters. The maximum CR momentum depends strongly on E_{sn} and M_{ej} , but is only weakly dependent upon the ISM density ρ_0 .

We note that a maximum proton momentum $p_{\text{max}} \sim 10^6 m_p c$ is required to reproduce the spectrum of Galactic CRs up to the knee energy (Berezhko & Ksenofontov 1999).

The maximum momentum in the overall CR spectrum, which is almost constant at the late epoch $t > 10^3$ yr, is about $p_{\text{max}} \approx 10^6 m_p c$ and corresponds to the beginning of the Sedov phase. All the very high-energy protons produced during the preceding free expansion phase $t < t_0$ contribute only a very steep power law tail at larger momenta $p > p_{\text{max}}$ in the final overall spectrum. The shape of this high energy tail can be derived as follows:

The kinetic energy of the ejecta contained in the fraction with speed v within the interval dv is

$$dE_{\text{ej}}(v) \propto v^{4-k} dv. \quad (23)$$

The CR spectrum created by the strongly modified shock is quite hard: $N(p) \propto p^{-\gamma}$, $\gamma < 2$. For the sake of a rough estimate we assume that all the above energy of the ejecta goes into CRs with maximum momenta $p_m(V_s)$, where the shock speed is roughly the speed $V_s \approx v$ of the ejecta. This gives

$$N(p_m) p_m dp_m \propto dE_{\text{ej}} \quad (24)$$

in the ultrarelativistic case. During the period of SNR evolution when the shock is already modified we have $B_0 \propto V_s$ and therefore $p_m \propto R_s V_s B \propto V_s^{2-\nu/(1-\nu)}$ so that we obtain $N \propto p^{-\gamma}$ with

$$\gamma = (9k - 33)/6. \quad (25)$$

For the case $k = 7$ this gives $\gamma = 5$ which agrees with the numerical results (Fig. 2). This consideration shows the following: despite the fact that during the free expansion phase the SN shock produces CRs with a power law spectrum up to the momentum $p_m(t_0)$ which is larger than what is attained in the Sedov phase, $p_m(t > t_0)$, these particles are seen only in a very steep part of the final overall CR spectrum due to their low number (low energy content). In addition, significant shock modification does not start at the very beginning of SNR evolution but only at $t \gtrsim 100$ yr. Due to the fact that efficient CR production (followed by strong shock modification and magnetic field amplification) takes place only during a relatively short period in the free expansion phase, this power law spectrum ends in an exponential cutoff at a momentum which is only a factor of 3 larger than p_{max} . Basically these particles play no role for the population of Galactic CRs. We should add here that in the case of type II and Ib SNe, which are more numerous in our Galaxy (Tammann et al. 1994), the value of the parameter k is even larger, $k \approx 10$ (e.g. Chevalier & Fransson 1984). In these cases the free expansion phase presumably contributes even less to the final CR spectrum.

4.2. Electron distribution

At low momenta we have $N_e(p) \propto N(p)$. However, the shape of the overall electron spectrum deviates from that of the proton spectrum at high momenta $p > p_1 \approx 10^3 m_p c$ due to the synchrotron losses in the downstream magnetic field which is assumed uniform ($B_d = B_2 = \sigma B_0$). According to expression (6) the synchrotron losses become important for electron momenta greater than

$$\frac{p_1}{m_p c} \approx \left(\frac{10^8 \text{ yr}}{t} \right) \left(\frac{10 \mu\text{G}}{B_d} \right)^2. \quad (26)$$

The shock continues to produce an electron spectrum $f_e \propto p^{-q}$ with $q \approx 4$ up to a maximum momentum p_{max}^e which is significantly larger than p_1 . In the momentum range from p_1 to p_{max}^e , due to the synchrotron losses the overall electron spectrum is therefore close to $N_e \propto p^{-3}$.

The maximum electron momentum can be estimated by equating the synchrotron loss time with the acceleration time. This results in (e.g. Berezhko et al. 2002)

$$\frac{p_{\text{max}}^e}{m_p c} = 6.7 \times 10^4 \left(\frac{V_s}{10^3 \text{ km s}^{-1}} \right) \times \sqrt{\frac{(\sigma - 1)}{\sigma(1 + \sigma^2)} \left(\frac{10 \mu\text{G}}{B_0} \right)}. \quad (27)$$

The main fraction of the electrons with the highest energies $p \sim 10^5 m_p c$ is produced at the end of the free expansion phase. In this stage, according to Fig. 1a, $V_s \sim V_0 = 8.5 \times 10^3 \text{ km s}^{-1}$ and

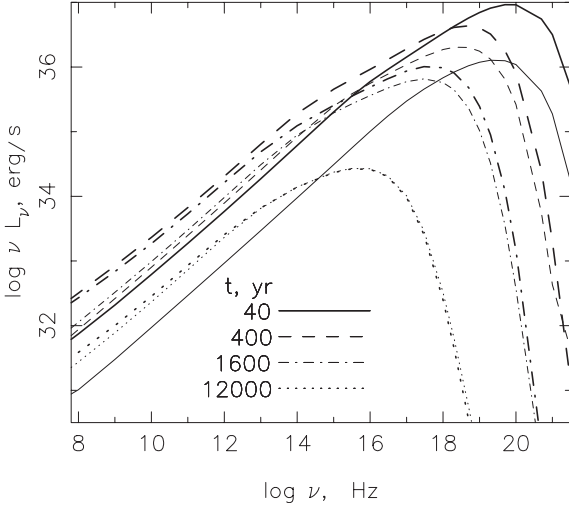


Fig. 3. Synchrotron spectral luminosity distribution as a function of frequency at four different times, for the same case as in Fig. 2 (thin lines). Thick lines correspond to the injection parameter value $\eta = 3 \times 10^{-4}$.

$B_0 \approx 30 \mu\text{G}$, which leads to a maximum electron momentum $p_{\text{max}}^e \approx 4 \times 10^5 m_p c$, in agreement with the numerical results (Fig. 2).

5. Synchrotron luminosity

To illustrate the time variation of the synchrotron spectrum during the SNR evolution we present in Fig. 3 the calculated synchrotron luminosity $L_\nu(\nu)$ in an ISM with number density $N_H = 0.3 \text{ cm}^{-3}$, for different ages. The shape of the spectrum $L_\nu(\nu)$ is directly related to the overall electron spectrum $N_e(p)$, shown in Fig. 2. For relatively low frequencies $\nu < 10^{14} \text{ Hz}$ it has a power law form

$$L_\nu \approx A_\nu B^{\alpha+1} \nu^{-\alpha}, \quad (28)$$

where the power law index $\alpha = (\gamma - 1)/2$ is related to the power law index γ which determines the electron spectrum $N_e \approx A_e p^{-\gamma}$ near the electron momentum

$$\frac{p}{m_e c} = \left(\frac{4\pi m_e c^2 \nu}{0.87 e c B_\perp} \right)^{1/2}, \quad (29)$$

which gives the maximum contribution to the synchrotron emission at frequency ν . Due to the shock modification the electron spectrum has a concave shape characterized by an index γ which slowly decreases with increasing energy. Therefore the synchrotron spectrum also has a concave shape with $\alpha > 0.5$ at the lowest frequencies $\nu \sim 1 \text{ GHz}$, decreasing to $\alpha = 0.5$ at $\nu \gg 1 \text{ GHz}$ (e.g. Reynolds & Ellison 1992; Berezhko et al. 2002).

The current luminosity L_ν is determined by the downstream magnetic field value at the current epoch $B_d \approx \sigma B_0$, which decreases with time due to the shock deceleration, and by the total number of electrons produced during all the previous stages $A_\nu \propto A_e$. During the initial period, $t < 10^3 \text{ yr}$, the factor $A_\nu \propto A_e$ grows more rapidly than the factor $B^{\alpha+1}$ decreases and this leads to an increase of L_ν in this period. In the later epoch

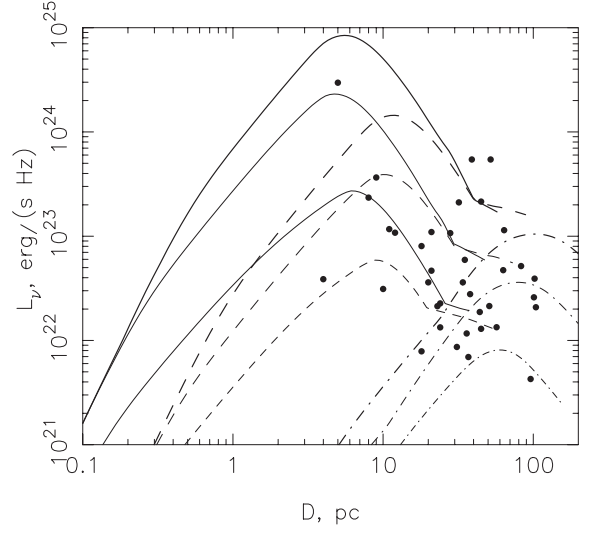


Fig. 4. The radio spectral luminosity distribution at $\nu = 1 \text{ GHz}$ as a function of SNR diameter in the case of SNR with explosion energy $E_{\text{sn}}/(10^{51} \text{ erg}) = 0.25$ (thin lines), 1 (normal) and 3 (thick) in an ISM of density $N_H/(1 \text{ cm}^{-3}) = 3$ (solid lines), 0.3 (dashed) and 0.003 (dash-dotted). Observational data, comprising 37 Galactic SNRs of known distances, are shown (Case & Bhattacharya 1998).

$t > 2 \times 10^3 \text{ yr}$ the number of accelerated electrons increases only slowly with time. Therefore the decrease of the magnetic field strength leads to a decrease of L_ν .

The synchrotron emission at the highest frequencies $\nu > 10^{14} \text{ Hz}$ is produced by the electrons with $p > p_1$, which suffer dramatic synchrotron cooling. Therefore, in addition to the above physical factors, the behavior of the synchrotron spectrum L_ν in this frequency range is influenced by the values of $p_1(t)$ and $p_{\text{max}}^e(t)$. Taking into account expression (27) for the electron cutoff momentum and relation (29), one can easily derive the value of the cutoff frequency

$$\nu_{\text{max}} = 2.1 \times 10^{17} b_\perp \frac{\sigma - 1}{\sigma^2 + 1} \left(\frac{V_s}{10^3 \text{ km s}^{-1}} \right)^2 \text{ Hz}, \quad (30)$$

where $b_\perp = B_{d\perp}/B_d$. It is taken as $b_\perp = 0.5$ in our calculation. Since the cutoff frequency is mainly determined by the shock speed, its value ν_{max} goes down quickly during the SNR evolution due to the shock deceleration, as seen from Fig. 3. It is interesting to note that at frequency $\nu \sim 10^{18} \text{ Hz}$, corresponding to the typical hard X-ray energy $\epsilon_\nu = 4 \text{ keV}$, only relatively young SNRs of age $t \lesssim 10^3 \text{ yr}$ produce very intense nonthermal X-ray emission which belongs to the power law part of the synchrotron spectrum $L_\nu(\nu)$. Over the subsequent epochs $t \gtrsim 10^3 \text{ yr}$ the shock speed becomes so small that the above X-ray frequency range falls into to the exponential tail of the spectrum. This leads to a fast decrease of the nonthermal X-ray emission during this period of SNR evolution.

To illustrate the evolution of the synchrotron flux we present in Fig. 4 the luminosity L_ν at $\nu = 1 \text{ GHz}$ as a function of SNR diameter for the case of SNRs with explosion energy $E_{\text{sn}}/(10^{51} \text{ erg}) = 0.25, 1$ and 3 in an ISM of density $N_H/(1 \text{ cm}^{-3}) = 0.003, 0.3$ and 3 .

The variation of the synchrotron flux is due to variation of R_s , V_s and B .

During a short initial period, which lasts from $t \approx 1$ yr for $N_H = 3 \text{ cm}^{-3}$ to $t \approx 10$ yr for $N_H = 0.003 \text{ cm}^{-3}$ (see Fig. 1a), the SN shock speed is constant. Since the SNR shock is not significantly modified in the free expansion phase (see Fig. 1b), the CR distribution function at the shock front has the form

$$f_s = \frac{4\eta N_H}{4\pi p_{\text{inj}}^3} \left(\frac{p}{p_{\text{inj}}} \right)^{-4}, \quad (31)$$

which shows that the CR number density at the shock front is proportional to the momentum $p_{\text{inj}} \propto V_s$ of the suprathermal particles injected at the shock front into the acceleration process. Therefore we have $A_e \propto N_H V_s R_s^3$, $B_d \propto \sqrt{N_H}$ and

$$L_\nu \propto N_H^{7/4} D^3, \quad (32)$$

taking into account that in the case of an unmodified shock $\gamma = 2$ and $\alpha = 0.5$. This explains the rising part of the calculated curves $L_\nu(D)$ which corresponds to small diameter values D in Fig. 4.

During the subsequent part of the free expansion phase the SN shock decelerates. According to Eq. (13) its speed as a function of shock radius is

$$V_s \propto \left[E_{\text{sn}}^2 / (M_{\text{ej}} N_H) \right]^{1/4} R_s^{-3/4}. \quad (33)$$

Since the shock, as in the previous epoch, is not yet strongly modified, the CR pressure goes like $P_c \propto N_H V_s$, leading to a magnetic field variation $B_d \propto \sqrt{N_H V_s}$. The expected luminosity dependence on the SNR diameter is then

$$L_\nu \propto \left(E_{\text{sn}}^2 / M_{\text{ej}} \right)^{7/16} N_H^{21/16} D^{27/16}, \quad (34)$$

which rather well explains the $L_\nu(D)$ dependence for $D < D_0 = 2R_0$.

In the subsequent Sedov phase a substantial fraction of the total energy E_{sn} goes into the CR component whose overall number remains nearly constant so that $A_e \propto E_{\text{sn}}$. Note that the ISM density N_H influences the amplified magnetic field value B_0 , which in turn influences the shock modification and CR acceleration efficiency (see Fig. 1). But this influence is not very significant: as one can see from Fig. 1 an increase of N_H by a factor of 10^3 leads to an increase of E_c by a factor of only two. Therefore, for a rough estimate, E_c and $A_e \propto E_c$ can be considered as independent of N_H . In this stage the SN shock is significantly modified. This is a consequence of the fact that the CR pressure is an important fraction of the shock ram pressure, with $P_c \propto \rho_0 V_s^2$. The downstream magnetic field $B_d \propto \sigma \sqrt{P_c}$ also varies due to the variation of the shock compression ratio σ . Since the variation of σ is much weaker than that of P_c , we can neglect it for qualitative analysis, taking $B_d \propto \sqrt{P_c} \propto \sqrt{N_H} V_s$. Then, taking into account the expansion law (14) we have

$$L_\nu \propto E_{\text{sn}}^{7/4} D^{-9/4} \quad (35)$$

independently of N_H and M_{ej} , if for simplicity we again assume the electron spectrum $N_e \propto p^{-\gamma}$ with power law index $\gamma = 2$, which implies $\alpha = 0.5$. The calculated electron spectra corresponding to the Sedov phase are steeper due to the shock modification. This implies $\gamma > 2$ at those energies which are responsible for the radio emission. In addition, the power law index

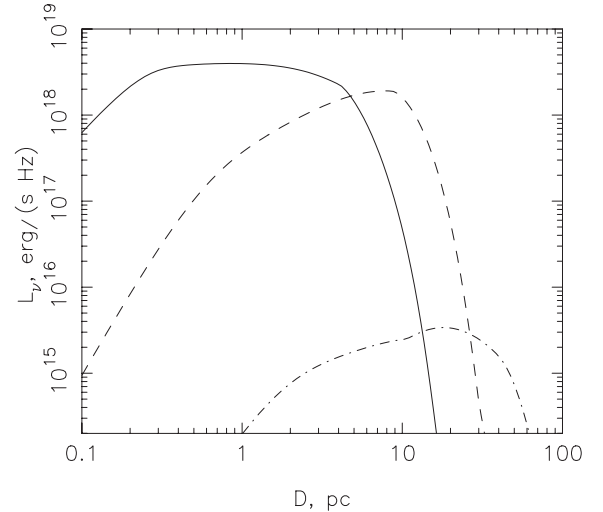


Fig. 5. The X-ray spectral luminosity distribution at $\nu = 10^{18}$ GHz (photon energy $\epsilon_\nu = 4$ keV) as a function of SNR diameter in the case of a SNR with explosion energy $E_{\text{sn}} = 10^{51}$ erg in an ISM of density $N_H/(1 \text{ cm}^{-3}) = 3$ (solid line), 0.3 (dashed line) and 0.003 (dash-dotted line).

γ varies during shock evolution and therefore the dependencies $L_\nu(D)$ are not of a pure power law nature, as is seen from Fig. 4, especially in the case of a dense ISM with $N_H \gtrsim 0.1 \text{ cm}^{-3}$ when the shock modification is most significant. Nevertheless the above analytical relation can be used for rough estimates.

In the late Sedov phase, when the effective magnetic field drops to $B_0 = B_{\text{ISM}}$ and remains constant thereafter, the expected SNR luminosity $L_\nu \propto E_{\text{sn}}$ is roughly independent of D .

As pointed out by Case & Bhattacharya (1998), there exists no significant correlation between radio luminosity and linear diameter. If SNe are more or less uniformly distributed over the considered range of ISM densities then it is clear from Fig. 4 that no significant correlation between L_ν and D is to be expected. At least the sample of Case & Bhattacharya appears to be uniformly distributed.

According to the calculated dependence of L_ν on D almost all observed SNRs are at the very end of their free expansion phase or in the Sedov phase. If this is generally so, then the lack of data with small SNR sizes D which correspond to the ages $t \ll t_0$ is a consequence of the relatively low expected luminosity of SNRs of age $t \ll t_0$. In addition, it can also be due to a selection effect: SNRs with small size and low luminosity are more difficult to recognize.

At high frequencies $\nu \sim 10^{18}$ Hz, which correspond to the hard X-ray range, the decrease of the cutoff frequency ν_{max} becomes appreciable already for $t \gtrsim 100$ yr. This is why the luminosity $L_\nu(D)$ at $\nu = 10^{18}$ Hz, shown in Fig. 5, begins to decrease already in the early Sedov phase. This factor becomes dominant for $t > 10^3$ yr and leads to a very steep dependence $L_\nu(D)$. For this reason only relatively young SNRs in free expansion or in the early Sedov phase are likely to be detected in nonthermal X-rays. As is clear from Fig. 5, the relatively high synchrotron luminosity in X-rays, expected already during the free expansion phase, can help to identify very young SNRs that are not yet bright radio sources.

In order to study the sensitivity of our results to the injection rate we present in Figs. 1 and 3 for the case $E_{\text{sn}} = 10^{51}$ erg $N_{\text{H}} = 0.3 \text{ cm}^{-3}$ the calculations that correspond to the substantially higher injection rate $\eta = 3 \times 10^{-4}$. The influence of η is quite different in different SNR evolutionary stages. When the SN shock is not modified (linear CR acceleration regime), the shape of the CR spectrum does not depend on η and the amplitude of the spectrum is proportional to η . Such a situation results during the initial part of the free expansion phase: as can be seen from Fig. 1b, at $t \lesssim 10$ yr the shock is only slightly modified. Since $P_{\text{c}} \propto \eta$, the increase of η leads to an increase of the magnetic field value $B_0 \propto \sqrt{\eta}$ (Fig. 1a), and therefore the synchrotron luminosity (Fig. 3) increases by a factor of about 7 compared with the case $\eta = 10^{-4}$.

When the shock is already strongly modified, i.e. at the end of free expansion and in the Sedov phase, the relation between η and the characteristics of CRs in a SNR become more complicated. The shock modification and CR energy content, which are closely connected with each other, are relatively weakly sensitive to the injection rate as can be seen from Fig. 1. Similarly, the synchrotron luminosities corresponding to the two values of η considered progressively approach each other for $t \gtrsim 100$ yr, so that during the Sedov phase $t > 10^3$ yr the influence of η on $L_{\nu}(\nu)$ becomes very small (see Fig. 3). Note also that for a higher injection rate that leads to larger shock modification the synchrotron spectrum in the radio range becomes steeper due to the concave shape of the spectrum of accelerated CRs.

6. The Σ - D relations in the radio range

In Fig. 6 we present the surface brightness

$$\Sigma_{\nu} = L_{\nu} / (\pi^2 D^2) \quad (36)$$

at frequency $\nu = 1$ GHz as a function of SNR diameter $D = 2R_{\text{s}}$. In the sequel we shall use Σ_{R} for the brightness in the radio band and Σ_{X} for the X-ray band, respectively. Calculations were performed for the above three different ISM densities and for the three values of the SN explosion energy $E_{\text{sn}}/(10^{51}) \text{ erg} = 0.25, 1$ and 3 , respectively. It was assumed that this energy interval covers the majority of the observed SNRs. The experimental values corresponding to 37 Galactic shell SNR with known distances (Case & Bhattacharya 1998) and to SNRs in the Magellanic Clouds, M 31 and M 33 (Berkhuijsen 1986) are also shown in Fig. 6.

The relation $\Sigma_{\nu}(D)$ is a direct consequence of the $L_{\nu}(D)$ dependence. During the initial part of the free expansion phase according to Eq. (32) the expected dependence is

$$\Sigma_{\text{R}} \propto N_{\text{H}}^{7/4} D, \quad (37)$$

and explains very well the numerical $\Sigma_{\text{R}}(D)$ behavior for small D ($D < 0.2$ pc for $N_{\text{H}} = 3 \text{ cm}^{-3}$ and $D < 2$ pc for $N_{\text{H}} = 0.003 \text{ cm}^{-3}$) in Fig. 6. In this region Σ_{R} does not depend on the SN parameters E_{sn} and M_{ej} , but does very sensitively depend on the ISM density.

During the subsequent part of the free expansion phase the expected dependence is

$$\Sigma_{\text{R}} \propto (E_{\text{sn}}^2 / M_{\text{ej}})^{7/16} N_{\text{H}}^{21/16} D^{-5/16}, \quad (38)$$

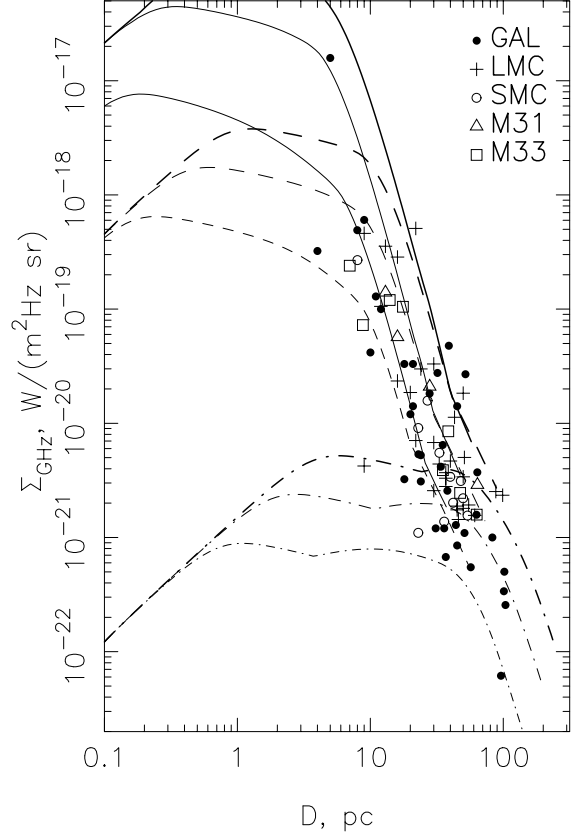


Fig. 6. Surface brightness-diameter diagram at frequency $\nu = 1$ GHz. Different styles of lines correspond to the same cases as in Fig. 4. Experimental data for the Galaxy (Case & Bhattacharya 1998) and for the Magellanic Clouds, M 31 and M 33 (Berkhuijsen 1986) are shown.

cf. Eq. (34). During this period of SNR evolution the surface brightness is very sensitive to the values of the explosion energy E_{sn} and of the ambient gas number density N_{H} , as can also be seen from Fig. 6.

In the subsequent Sedov phase, according to Eq. (35) we have

$$\Sigma_{\text{R}} \propto E_{\text{sn}}^{7/4} D^{-17/4}, \quad (39)$$

independent of N_{H} and M_{ej} . Since our magnetic field strength $B_{\text{d}} \propto V_{\text{s}}$ in the Sedov phase changes in a way similar to what was suggested by Reynolds & Chevalier (1981), the above $\Sigma_{\text{R}}(D)$ dependence is the same as they derived.

Note again that this dependence $\Sigma_{\text{R}} \propto D^{-17/4}$ is valid only for the electron spectrum $N_{\text{e}} \propto p^{-2}$ which is created by the unmodified shock. The actual shock during the Sedov phase, as can be seen from Fig. 1b, is significantly modified. The modification, characterized by the deviation of the shock and subshock compression ratios σ and σ_{s} from the classical value 4, is larger for denser ISM. Therefore the calculated dependence $\Sigma_{\text{R}}(D)$ presented in Fig. 6 is close to $\Sigma_{\text{R}} \propto D^{-17/4}$ in the case of a diluted ISM with number density $N_{\text{H}} = 0.003 \text{ cm}^{-3}$ for which the shock is only slightly modified (see Fig. 1b) and it becomes steeper with the increase of the ISM density.

In the late Sedov epoch, when due to the shock deceleration the magnetic field amplification becomes irrelevant, and

therefore the downstream SNR field becomes constant, the $\Sigma_R(D)$ dependence goes toward

$$\Sigma_R \propto E_{\text{sn}} N_{\text{H}}^{3/4} D^{-2}. \quad (40)$$

The fact that the observational data points lie in a relatively compact region on the $\Sigma_R - D$ diagram can be explained from a theoretical point of view if we suggest that nearly all of the identified SNRs with known distance are in the Sedov phase, or at least at the end of the free expansion phase. The lack of a significant number of SNRs detected in the early free expansion phase can be due to the small SNR size and correspondingly small synchrotron flux expected in this stage, as discussed before.

Even though the expected relation $\Sigma_R \propto E_{\text{sn}}^{7/4} D^{-17/4}$ does not depend on the ISM gas density, it is clear from Fig. 6 that for small diameters $D < 10$ pc only SNRs located in a dense ISM with $N_{\text{H}} > 1 \text{ cm}^{-3}$ are contained in the sample, whereas for the largest diameters $D > 30$ pc the dominant SNRs are those which are in a tenuous ISM with $N_{\text{H}} < 0.01 \text{ cm}^{-3}$. If in addition we assume that SNRs in the early Sedov phase are predominantly detected, then one would expect that the relation $D \propto N_{\text{H}}^{-1/3}$ is roughly valid, which leads to $\Sigma_R \propto N_{\text{H}}^{17/12}$ which agrees very well with the dependence determined from observations (Berkhuijsen 1986).

Note that type II and Ib SNe, whose number is expected to exceed the number of type Ia SNe considerably, are characterized by essentially different values of the mass of ejecta M_{ej} and of their initial velocity distribution. Nevertheless, in the Sedov phase this difference becomes irrelevant. Therefore we restrict our consideration here to type Ia SNe. On the other hand, according to expressions (33) and (34), in the free expansion phase the expected radio luminosity of type II and Ib SNe with typical ejecta masses between $M_{\text{ej}} = 5$ and $10 M_{\odot}$, is lower by a factor of two to three than that of type Ia SNe considered here.

In Figs. 4 and 6 the brightest object is Cas A, which is probably a type Ib SN with a Wolf-Rayet star progenitor, or possibly a type II SN. It is therefore not thought to genuinely belong to any of the evolutionary tracks shown. However, it remains true that the enormous radio luminosity and surface brightness of this young and rather small object can only be explained by a high-density environment, as suggested in these figures.

7. The $\Sigma - D$ relation in the X-ray range

During the last several years a number of SNRs have been discovered as sources of nonthermal X-rays (e.g. Petre et al. 2001). Studies of the spatial fine structures of the nonthermal X-ray emission from SNRs with high angular resolution instruments like Chandra (Hwang et al. 2002; Vink & Laming 2003; Long et al. 2003; Bamba et al. 2003) are extremely interesting, since the observed small scale structures yield decisive information about the actual magnetic field strength in these remnants. The most important conclusion is that in all cases the magnetic field strength derived from these observations are considerably higher than expected for typical ISM fields (Berezhko et al. 2003a; Berezhko & Völk 2004). Therefore it

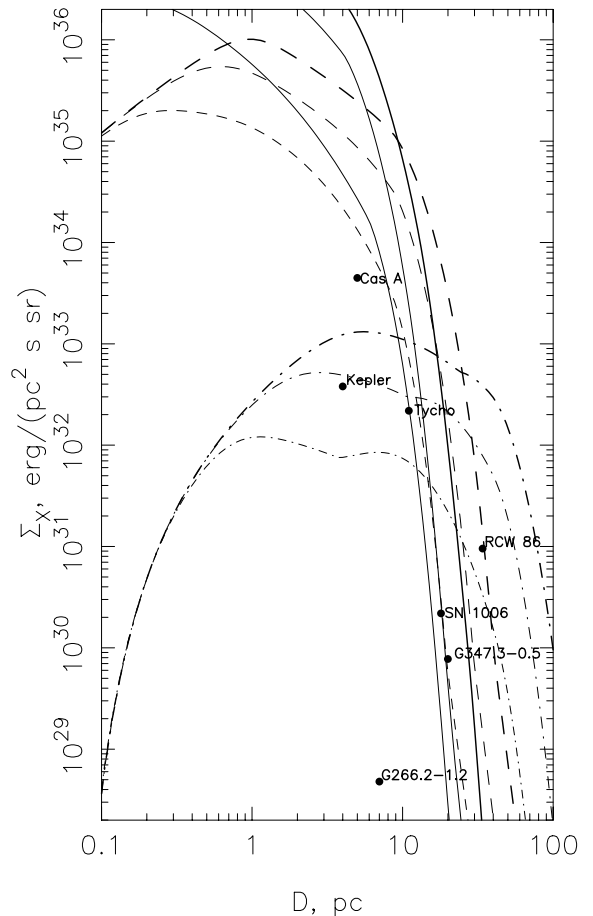


Fig. 7. The same as in Fig. 6 but for the frequency $\nu = 10^{18}$ Hz (photon energy $\epsilon_{\nu} \approx 4$ keV). Experimental values for seven Galactic SNRs (see text) are shown.

is worthwhile to study the synchrotron luminosity of SNRs in the X-ray band.

In Fig. 7 we show the surface brightness Σ_X at frequency $\nu = 10^{18}$ Hz (photon energy $\epsilon_{\nu} = 4$ keV) as a function of SNR diameter, for the same three values of ISM density and SN explosion energy as considered before. The experimental brightness calculated from the measured X-ray fluxes (and extrapolated to a given energy $\epsilon_{\nu} = 4$ keV) for Cas A, Tycho's SNR, RCW 86, Kepler and SN 1006 is taken from Petre et al. (2001), for G347.3-0.5 from Slane et al. (1999), and for G266.2-1.2 from Duncan & Green (2000). A distance $d = 1$ pc is taken for the last two objects.

In the free expansion phase the $\Sigma_X(D)$ dependence is very similar to that in the radio range because during this epoch the frequency is lower than the cutoff frequency ν_{max} (see Fig. 3), and therefore the X-ray luminosity is determined by the same factors as in the radio band.

A dramatically different situation exists for larger diameters ($D > 4, 8$ and 20 pc for $N_{\text{H}} = 1, 0.3$ and 0.003 cm^{-3} , respectively), which correspond to the Sedov phase. Due to the decrease of the cutoff frequency ν_{max} the frequency $\nu = 10^{18}$ Hz becomes larger than ν_{max} already at the beginning of this stage. This leads to a very rapid decrease of the synchrotron luminosity L_{ν} and of the brightness Σ_X . For example, the brightness Σ_X

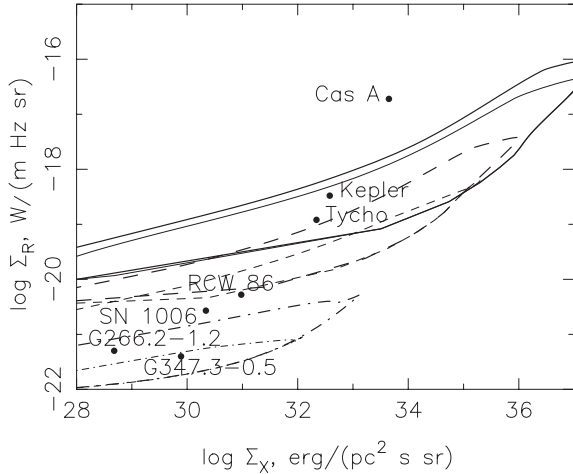


Fig. 8. Spectral surface brightness distribution at frequency $\nu = 1$ GHz versus surface brightness at $\nu = 10^{18}$ Hz (photon energy $\epsilon_\nu \approx 4$ keV) for the same cases as in Fig. 4, except that corresponding to $E_{\text{sn}} = 10^{51}$ erg.

becomes as low as 10^{29} erg/(pc² s sr) for $D = 20$ pc in the case $E_{\text{sn}} = 10^{51}$ erg and $N_{\text{H}} = 0.3$ cm⁻³ that corresponds to a relatively young SNR (see Fig. 1a) of age $t \approx 2 \times 10^3$ yr. It is therefore not surprising that the number of SNRs detected as sources of nonthermal X-rays is so small, and that all of these sources are young.

Since the radio and X-ray synchrotron emissivities of SNRs are of the same physical nature, it is interesting to study the relation to be expected between them. For this purpose the radio brightness $\Sigma_{1\text{GHz}}$ is plotted in Fig. 8 versus the X-ray SNR brightness Σ_{X} for the same ranges of the explosion energy E_{sn} and ISM number density N_{H} as before.

It is interesting to note that the allowed region in this $\Sigma_{\text{R}} - \Sigma_{\text{X}}$ diagram is very limited, especially if the ambient ISM density is known. This is because a relatively high X-ray brightness is expected for only a limited range of the SNR sizes, corresponding to the free expansion phase. In Fig. 8 all Galactic SNRs except Cas A are inside the expected region in the $\Sigma_{\text{R}} - \Sigma_{\text{X}}$ diagram. A possible explanation is again that Cas A is not a type Ia SNR, but certainly a type Ib or a type II SNR expanding into a nonuniform circumstellar medium strongly modified by the progenitor star wind. What is even more essential in this case is that the mass of the ejecta is substantially higher than in the case of a type Ia SN. This implies a lower shock speed for the same explosion energy than in the type Ia case. As was already pointed out, X-ray synchrotron emission is very sensitive to the shock speed. Lowering the shock speed will therefore shift the theoretical curve in Fig. 8 mainly to the left, toward lower values of Σ_{X} . This could lead to bounding the experimental Cas A point by the curve that corresponds to $N_{\text{H}} = 3$ cm⁻³. This mean density appears to be an appropriate value for Cas A.

8. Discussion and conclusions

The nonlinear kinetic theory for CR production in SNRs has been used for the first time in order to study the statistical

properties of the synchrotron emission of SNRs, in particular the $\Sigma - D$ relation.

Following the result of theoretical modeling of magnetic field amplification near the shock due to CRs (Luceck & Bell 2000), the theoretical analysis of the spectral properties of the nonthermal emission of individual SNRs (Berezhko et al. 2002, 2003b; Völk et al. 2002) which predicted magnetic field strengths inside young SNRs much larger than typical ISM values, and the experimental studies of the fine structure of nonthermal X-ray emission of young SNRs (Hwang et al. 2002; Vink & Laming 2003; Long et al. 2003; Bamba et al. 2003), we incorporate into our model a time-dependent magnetic field, whose energy density is proportional to the CR pressure. This effect influences the SNR synchrotron emission drastically, making it much more intense, especially in the case of relatively young SNRs.

Since the value of the magnetic field in the most active SNR phase for CR production, the early Sedov phase, is more than an order of magnitude larger than the ISM field, the overall CR proton power law spectrum, produced during the whole SNR evolution, extends up to an energy $\epsilon_{\text{max}} \approx 10^{15}$ eV, independent of the ISM density. This is just the condition required to explain the Galactic CR spectrum due to SNRs up to the energy of the knee, which is 3×10^{15} eV (Berezhko & Ksenofontov 1999).

The maximum energy of CR electrons is about an order of magnitude lower due to synchrotron losses. In addition, as a consequence of these losses, the electron spectrum is much steeper than the proton spectrum at energies $\epsilon_e \gtrsim 100$ GeV.

Reynolds & Keohane (1999) and Heindrich & Reynolds (2001) estimated the maximum electron energy for a number of galactic and extragalactic SNRs based on the measured radio and X-ray spectra. Their values of ϵ_{max}^e are within the range of from $10 \sqrt{10 \mu\text{G}/B_d}$ TeV to $200 \sqrt{10 \mu\text{G}/B_d}$ TeV, consistent with our predictions (see Figs. 2 and 1a).

It was shown that, as a result of the progressively increasing overall number of accelerated CRs, the radio synchrotron luminosity increases with time in the free expansion phase, achieves its peak value at the very beginning of the Sedov phase, and then again decreases with time due to the decreasing strength of the effective magnetic field. The dependence of the radio luminosity on the diameter, calculated for typical values of the ISM density and of the SN explosion energy, covers the region of the experimental points on the $L_\nu - D$ diagram very well. The lack of data for small linear sizes $D \ll 10$ pc is tentatively explained by a low luminosity in the free expansion phase that makes it difficult to recognize SNRs with small size and low luminosity.

In contrast to the radio range, the synchrotron luminosity in the X-ray range, which has its peak value at the beginning of the Sedov phase as well, goes down much more rapidly with increasing D , due to the decrease of the electron cutoff momentum. This determines the corresponding value of the cutoff synchrotron frequency.

The theory predicts a dependence of radio SNR brightnesses on diameter D which is close to $\Sigma_{\text{R}} = AD^{-17/4}$ in the Sedov phase. All the SNRs corresponding to the same explosion energy E_{sn} are expected to align along the same line

$\Sigma_R = AD^{-17/4}$, independent of ISM density. The amplitude of this dependence scales with the explosion energy according to $A \propto E_{\text{sn}}^{7/4}$. Therefore the variation of E_{sn} within a factor of ten, that has to be considered as an appropriate assumption for the actual Galactic SNR population, makes it possible to cover almost the whole region in the $\Sigma_R - D$ diagram by the lines $\Sigma_R = AD^{-17/4}$. The spread in SNR luminosities at a given SNR diameter D is mainly due to the spread of the explosion energy E_{sn} . It therefore provides the theoretical basis for the $\Sigma_R - D$ diagram as an instrument for the distance determination to SNRs.

The expected injection rate $\eta \sim 10^{-4}$ leads to significant SN shock modification as a result of the CR backreaction during the Sedov phase. Due to the strong nonlinear coupling at this stage the final results are relatively insensitive to η . The synchrotron luminosity is sensitive to η only during the initial part of the free expansion phase, when the shock is not modified, scaling roughly as $L_\nu \propto \eta^{7/4}$.

It is expected that SNRs in a dense ISM populate the part of the line $\Sigma_R = AD^{-17/4}$ which corresponds to low diameter values D , whereas SNRs in a diluted ISM are expected to be on this line for significantly larger D . This is an explanation for the empirical correlation $\Sigma_R \propto N_{\text{H}}^{1.37}$ between the radio brightness Σ_R and the ISM number density N_{H} (Berkhuijsen 1986). Since the scale value R_0 for the SNR size is proportional to $N_{\text{H}}^{1/3}$, the expected correlation is $\Sigma_R \propto N_{\text{H}}^{17/12}$. It agrees with the experimental relation in a very satisfactory way.

Acknowledgements. This work has been supported in part by the Russian Foundation for Basic Research (grant 03-02-16524). E.G.B. acknowledges the hospitality of the Max-Planck-Institut für Kernphysik where part of this work was carried out.

References

- Bamba, A., Yamazaki, R., Ueno, M., & Koyama, K. 2003, *ApJ*, 589, 827
- Bell, A. R. 1978, *MNRAS*, 182, 147
- Bell, A. R., & Lucek, S. G. 2001, *MNRAS*, 321, 433
- Bennet, L., & Ellison, D. C. 1995, *JGR*, 100, 3439
- Berezhko, E. G., & Krymsky, G. F. 1988, *Sov. Phys. Uspekhi*, 12, 155
- Berezhko, E. G. 1996, *Astropart. Phys.*, 5, 367
- Berezhko, E. G., Elshin, V. K., & Ksenofontov, L. T. 1996, *JETPh*, 82, 1
- Berezhko, E. G., & Völk, H. J. 1997, *Astropart. Phys.*, 7, 183
- Berezhko, E. G., & Ellison, D. C. 1999, *ApJ*, 526, 385
- Berezhko, E. G., & Ksenofontov, L. T. 1999, *JETPh*, 89, 391
- Berezhko, E. G., Ksenofontov, L. T., & Völk, H. J. 2002, *A&A*, 395, 943
- Berezhko, E. G., Ksenofontov, L. T., & Völk, H. J. 2003a, *A&A*, 412, L11
- Berezhko, E. G., Pühlhofer, G., & Völk, H. J. 2003b, *A&A*, 400, 971
- Berezhko, E. G., & Völk, H. J. 2004, *A&A*, 419, L27
- Berezinskii, V. S., Bulanov, S. A., Dogel, V. A., et al. 1990, *Astrophysics of cosmic rays* (North-Holland: Publ. Comp.)
- Bernhuijsen, E. M. 1987, *A&A*, 166, 257
- Blandford, R. D., & Ostriker, J. P. 1978, *ApJ*, 221, L29
- Blandford, R. D., & Eichler, D. 1987, *Phys. Rep.*, 154, 1
- Case, G. L., & Bhattacharya, D. 1998, *ApJ*, 504, 761
- Chevalier, R. A. 1974, *ApJ*, 188, 501
- Chevalier, R. A. 1982, *ApJ*, 258, 790
- Chevalier, R. A., & Fransson, C. 1984, *ApJ*, 420, 268
- Drury, L'O. C. 1983, *Rep. Progr. Phys.*, 46, 973
- Duric, N., & Seaquist, E. R. 1986, *ApJ*, 301, 308
- Duncan, A. R., & Green, D. A. 2000, *A&A*, 364, 732
- Dwarkadas, V. V., & Chevalier, R. A. 1998, *ApJ*, 497, 807
- Fedorenko, V. N. 1983, in *Supernova Remnants and their X-ray Emission*, ed. J. Danziger, & P. Gorenstein (Dordrecht: Reidel), IAU Symp., 101, 183
- Green, D. A. 1984, *MNRAS*, 209, 449
- Huang, Z. P., Thun, T. X., Chevalier, R. A., et al. 1994, *ApJ*, 424, 114
- Hwang, U., Decourshelle, A., Holt, S. S., & Petre, R. 2002, *ApJ*, 581, 1101
- Heindrich, S. P., & Reynolds, S. P. 2001, *ApJ*, 559, 903
- Jones, E. M., Smith, B. W., & Straka, W. C. 1981, *ApJ*, 249, 185
- Koyama, K., Petre, R., Gotthelf, E. V., et al. 1995, *Nature*, 378, 255
- Long, K. S., Reynolds, S. P., Raymond, J. C., et al. 2003, *ApJ*, 586, 1162
- Lucek, S. G., & Bell, A. R. 2000, *MNRAS*, 314, 65
- Malkov, M. A. 1998, *Phys. Rev. E*, 58, 4911
- Malkov, M. A., & Völk, H. J. 1995, *A&A*, 300, 605
- McKenzie, J. F., & Völk, H. J. 1982, *A&A*, 116, 191
- Mestel, L. 1965, *Quart. J. Roy. Astr. Soc.*, 6, 161, 265
- Petre, R., Hwang, U., & Allen, G. E. 2001, *Adv. Space Sci.*, 27, 647
- Ptuskin, V. S., & Zirakashvili, V. N. 2003, *A&A*, 403, 1
- Reynolds, S. P., & Chevalier, R. A. 1981, *ApJ*, 245, 912
- Reynolds, S. P., & Ellison, D. C. 1992, *ApJ*, 399, L75
- Reynolds, S. P., & Keohane, J. W. 1999, *ApJ*, 525, 368
- Scholer, M., Trattner, K. J., & Kucharek, H. 1992, *ApJ*, 395, 675
- Slane, P., Gaensler, B. M., Dame, T. M., et al. 1999, *ApJ*, 525, 357
- Tammann, G. A., Löffler, W., & Schröder, A. 1994, *ApJ*, 92, 487
- Trattner, K. J., & Scholer, M. 1994, *JGR*, 99, 6637
- Vink, J., & Laming, J. M. 2003, *ApJ*, 548, 758
- Völk, H. J., Berezhko, E. G., Ksenofontov, L. T., & Rowell, G. P. 2002, *A&A*, 396, 971
- Völk, H. J., Berezhko, E. G., & Ksenofontov, L. T. 2003, *A&A*, 409, 563

Online Material

Appendix A:

We consider here the spatial dependence of the effective downstream magnetic field B_d in the SNR interior.

Since the spatial scales of the amplified magnetic field are much smaller than the shock radius R_s , the field can be considered random and isotropic. Assuming it to be frozen into the thermal gas in the downstream region $r < R_s$, one can write (e.g. Mestel 1965; Chevalier 1974):

$$P_B \rho^{-4/3} = \text{const.}, \quad (\text{A.1})$$

where $P_B = B^2/(8\pi)$ is the magnetic pressure. Therefore at any given radial distance r we have

$$P_B(r, t) \propto P_{B2}(t_s) \rho(r, t)^{4/3}, \quad (\text{A.2})$$

where t_s is the instant of time when the gas element, at the present time $t > t_s$ located at radius r , had intersected the shock front, $r(t_s) = R_s(t_s)$. The postshock gas density ρ_2 is approximated by a constant value $\rho_2 = 4\rho_0$, where ρ_0 is the preshock density.

The profile of the downstream mass velocity $w(r, t)$ and density $\rho(r, t)$ of the gas in the Sedov phase can be approximated by $w = 3rV_s/(4R_s)$ and $\rho = 4\rho_0(r/R_s(t))^9$, neglecting here the shock modification by the CR backreaction. The shock radius R_s and the shock velocity V_s are given by $R_s \propto t^{2/5}$ and $V_s(t_s) \propto t_s^{-3/5}$, respectively. Therefore the equation of motion of a gas element

$$dr/dt = w(r, t) \quad (\text{A.3})$$

integrates to

$$r/R_s(t) = (t_s/t)^{1/10}, \quad (\text{A.4})$$

which gives $t_s \propto r^{10}/t^3$.

Substituting $P_{B2}(t_s) \propto V_s^2(t_s) \propto t_s^{-6/5}$ and $t_s(r, t)$ into Eq. (A.2), we find that the strong decrease of $\rho^{2/3} \propto r^6$ into the interior, where fluid elements shocked in the past are located, is compensated by the strong increase of V_s in the same past, i.e. that $B_d(r, t) = B_2(t)$. Thus $B_d(r, t)$ is uniform in this approximation.